NEOPLASIA
www.neoplasia.com

Volume 12 Number 12 December 2010 pp. 1054–1065 1054

Noninvasive Detection of Inflammation-Associated Colon Cancer in a Mouse Model[1]

Aaron C. Ericsson*, Matthew Myles*, Wade Davis†,‡, Lixin Ma§,¶, Michael Lewis¶, Lillian Maggio-Price# and Craig Franklin*

*Research Animal Diagnostic Laboratory, Department of Veterinary Pathobiology, University of Missouri, Columbia, MO, USA; †Department of Health Management and Informatics, University of Missouri, Columbia, MO, USA; ‡Department of Statistics, University of Missouri, Columbia, MO, USA; §Department of Radiology, University of Missouri, Columbia, MO, USA; ¶Harry S. Truman Memorial Veterans' Hospital, Columbia, MO, USA; #Department of Comparative Medicine, University of Washington, Seattle, WA, USA

Abstract

Helicobacter bilis–infected Smad3$^{-/-}$ mice represent an attractive model of inflammation-associated colon cancer. Most infected mice develop mucinous adenocarcinoma (MUC) by 6 weeks post inoculation (PI); however, approximately one third do not progress to MUC. The ability to predict the development of MUC in mice used in therapeutic studies would confer a considerable saving of time and money. In addition, the inadvertent use of mice without MUC may confound therapeutic studies by making treatments seem falsely efficacious. We assessed both magnetic resonance imaging (MRI) and fecal biomarkers in *Helicobacter*- and sham-inoculated mice as methods of noninvasively detecting MUC before the predicted onset of disease. Non–contrast-enhanced MRI was able to detect lesions in 58% of mice with histologically confirmed MUC; however, serial imaging sessions produced inconsistent results. MRI was also a labor- and time-intensive technique requiring anesthesia. Alternatively, inflammatory biomarkers isolated from feces at early time points were correlated to later histologic lesions. Fecal expression of interleukin 1β, macrophage inflammatory protein 1α, and regulated on activation, normal T-cell expressed, and secreted at 3 weeks PI correlated significantly with lesion severity at 9 weeks PI. For each biomarker, receiver-operator characteristic curves were also generated, and all three biomarkers performed well at 1 to 3 weeks PI, indicating that the development of MUC can be predicted based on the early expression of certain inflammatory mediators in feces.

Neoplasia (2010) 12, 1054–1065

Abbreviations: AUC, area under the curve: an overall indication of the diagnostic accuracy of a receiver-operator characteristic curve; CRC, colorectal cancer: a malignant neoplastic disease of the colon and/or rectum; HPRT, hypoxanthine guanine phosphoribosyltransferase: a constitutively produced enzyme involved in purine metabolism used to normalize the expression of other inducible proteins in polymerase chain reaction assays; IL-1β, interleukin 1β: a pleiotropic inflammatory cytokine produced by antigen-presenting cells and epithelial cells; MCP-2, monocyte chemotactic protein 2: a CC-type chemokine (CCL8) involved in mixed leukocyte recruitment and activation; MIP-1α, macrophage inflammatory protein 1: a CC-type chemokine (CCL3) involved in mixed leukocyte recruitment and activation; MUC, mucinous adenocarcinoma: a malignant growth of glandular epithelium retaining a glandular growth pattern microscopically, and producing significant amounts of mucin, accounting for approximately 11 to 15% of human colorectal adenocarcinoma; PI, post inoculation; RANTES, regulated on activation, normal T-cell expressed, and secreted: a CC-type chemokine (CCL5) involved in mixed leukocyte recruitment and activation; ROC, receiver-operator characteristic: a plot of the true-positive rate (sensitivity) against the false-positive rate (1 – specificity) for the different possible cutoff points of a diagnostic test; RT-PCR, reverse transcription–polymerase chain reaction: a variant of polymerase chain reaction used to amplify complementary DNA, which is initially generated from RNA using the enzyme reverse transcriptase; SROC, Spearman rank order correlation: a nonparametric measure of statistical dependence between two variables

Address all correspondence to: Craig Franklin, DVM, PhD, dACLAM, 4011 Discovery Dr, Columbia, MO 65201. E-mail: franklinc@missouri.edu

[1]This research was funded by National Institutes of Health grant K26 RR018811, National Institutes of Health training grant 5T32 RR007004-32, a grant from the Crohn's and Colitis Foundation of America (grant no. 1579 to L.M.P.), and a grant from the University of Missouri College of Veterinary Medicine Committee on Research.
Received 2 July 2010; Revised 3 September 2010; Accepted 9 September 2010

DOI 10.1593/neo.10940

Introduction

Colorectal cancer (CRC) is the second leading cause of cancer mortality in the United States, and the third most common type of cancer in men and women [1]. Along with certain hereditary conditions, inflammatory bowel disease (IBD) ranks as one of the top three high-risk conditions for CRC [2]. For IBD-associated CRC, there is no well-defined genetic cause, and CRC is thought to develop from a hyperplastic or dysplastic precursor lesion as a sequela to chronic inflammation. Classically, the stage of disease at diagnosis, as established by Dukes in 1932 [3], provides a prognostic indicator of survival [4] because resection before lymph node metastasis is often curative. Alternatively, diagnosis of CRC using Dukes' stage C or higher, indicating lymph node metastasis, is associated with poor 5-year survival rates, demonstrating the necessity of early detection. Currently, the most commonly used screening techniques are fecal occult blood testing (FOBT), sigmoidoscopy, colonoscopy, and computed tomographic (CT) colonography (often called virtual colonoscopy), all of which possess both advantages and disadvantages. FOBT is affordable and noninvasive, but it fails to detect most early precancerous polyps and some cancerous lesions in humans [5,6]. The endoscopic techniques can be used to biopsy or completely remove potential lesions at the time of the procedure; however, they require cleansing of the colon, sedation in the case of colonoscopy, and there is an inherent risk, albeit minimal, of damage to the mucosa. In addition, sigmoidoscopy is unable to detect lesions in the proximal colon [7]. CT colonography also requires cleansing of the colon. Mouse models of CRC are posed with similar challenges, particularly in the setting of therapeutic studies. As in humans, FOBT testing is limited by the same lack of robust sensitivity and specificity, and although colonoscopy is possible in mice [8,9], it is both time- and cost-intensive and requires anesthesia and substantial expertise.

Helicobacter-infected Smad3 knockout mice represent an attractive animal model for the study of CRC. Mice deficient in Smad3, a transcription factor downstream of the anti-inflammatory and pro-apoptotic cytokine transforming growth factor β, develop only a few mild phenotypic abnormalities including megaesophagus and, at a very low incidence, angular limb deformities [10] when raised in specific pathogen-free conditions. However, when infected with enterohepatic species of *Helicobacter*, e.g., *Helicobacter bilis* or *Helicobacter hepaticus* [11], approximately two-thirds of these mice develop mucinous adenocarcinoma (MUC) of the proximal colon by as early as 6 weeks post inoculation (PI). *H. bilis* and *H. hepaticus* induce intestinal inflammation in susceptible strains of mice [12,13], and the neoplasia seen in *Helicobacter*-infected Smad3$^{-/-}$ mice is considered a postinflammatory phenomenon [11]. In addition, loss of normal transforming growth factor β signaling is widely recognized as an indicator of malignancy in human CRC [14,15]. Thus, the targeted deletion of Smad3 in mice is a biologically relevant model of the human condition.

This model is ideal for therapeutic studies of CRC in that most mice develop disease on a predicted time course. Moreover, cancer develops in its natural setting as opposed to the more commonly used models that use flank injections of immunocompromised mice with human cancer cell lines. To enhance the usefulness of this model, it would be ideal to be able to identify CRC at early stages of disease or even before disease onset. This would allow for both the elimination of mice from expensive therapeutic studies as well as the assessment of therapeutics at various stages of disease. For the purposes of evaluating therapeutic compounds for the treatment of CRC, we endeavored to establish a method of screening *H. bilis*–infected Smad3$^{-/-}$ mice before the time at which disease typically occurs. Our goal was to refine this mouse model of CRC in an effort to reduce animal numbers and the associated costs and to increase the power of the data generated in these trials. Toward these ends, we evaluated both magnetic resonance imaging (MRI) and several fecal RNA biomarkers as means of detecting disease and predicting disease severity in *H. bilis*– and sham-inoculated Smad3$^{-/-}$ mice in two separate, sequential longitudinal studies using different cohorts of mice. MRI was selected, as opposed to CT, based on the greater soft tissue definition afforded by this modality. Non–contrast-enhanced MRI was able to detect MUC lesions beginning at 8 weeks PI, and 58% of mice with histologically confirmed lesions were correctly identified at 16 weeks PI. However, serial images produced inconsistent results. In addition, MRI requires considerable resources to perform, and image interpretation is inherently subjective and requires expertise. Alternatively, fecal expression of messenger RNA (mRNA) specific for interleukin 1β (IL-1β), macrophage inflammatory protein 1α (MIP-1α), and regulated on activation, normal T-cell expressed, and secreted (RANTES) at 3 weeks PI correlated significantly with MUC lesion severity at 9 weeks PI in *H. bilis*–infected Smad3$^{-/-}$ mice, allowing the identification of which mice have a high probability of developing MUC.

Materials and Methods

Bacteria and Cultivation

A *H. bilis* isolate was obtained from an endemically infected mouse colony using a previously described culture technique [16]. The isolate was identified as *H. bilis* based on ultrastructural morphology, biochemical characteristics, and sequence analysis of the 16S ribosomal RNA gene [17]. For inoculation, *H. bilis* cultures were grown in 5 ml of *Brucella* broth (Becton Dickinson, Franklin Lakes, NJ) supplemented with 5% fetal calf serum (Sigma-Aldrich Co, St Louis, MO) and overlaid on blood agar plates and incubated for 24 to 48 hours at 37°C in a microaerobic environment containing 90% N_2, 5% H_2, and 5% CO_2.

Animals

All studies were performed in accordance with the *Guide for the Care and Use of Laboratory Animals* and were approved by the University of Missouri Institutional Animal Care and Use Committee. 129-*Smad*$^{3tm/Par}$/J (referred to as Smad3$^{-/-}$) mice were bred on site for these studies. Mice were confirmed to be free of adventitious viruses, parasites, and pathogenic enteric and respiratory bacteria, including all known murine *Helicobacter* spp. Three- to four-week-old Smad3$^{-/-}$ mice were inoculated twice, 24 hours apart, with 10^8 *H. bilis* organisms in 0.5 ml of *Brucella* broth, or an equivalent volume of sterile broth, through gastric gavage. Separate cohorts of mice were used for each study including incidence of CRC (n = 5-9 mice per time point; Figures 1 and 2), MRI (n = 6 of each sex infected with *H. bilis* and n = 1 of each sex sham-infected; Figure 3), 9 weeks PI fecal mRNA levels (n = 7 *H. bilis*–infected and 9 sham-infected; Figure 4), and 1 to 7 weeks PI fecal mRNA levels (n = 14 of *H. bilis*–infected and n = 9 of sham-infected; Figures 5 and 6). Mice were group-housed according to infection status in autoclaved microisolator cages and were provided autoclaved food and water. All manipulations and sample collections were performed in a biosafety hood except for MRI. Mice were killed at 16 or 9 weeks PI for the MRI and fecal biomarker studies, respectively, through inhaled overdose of CO_2.

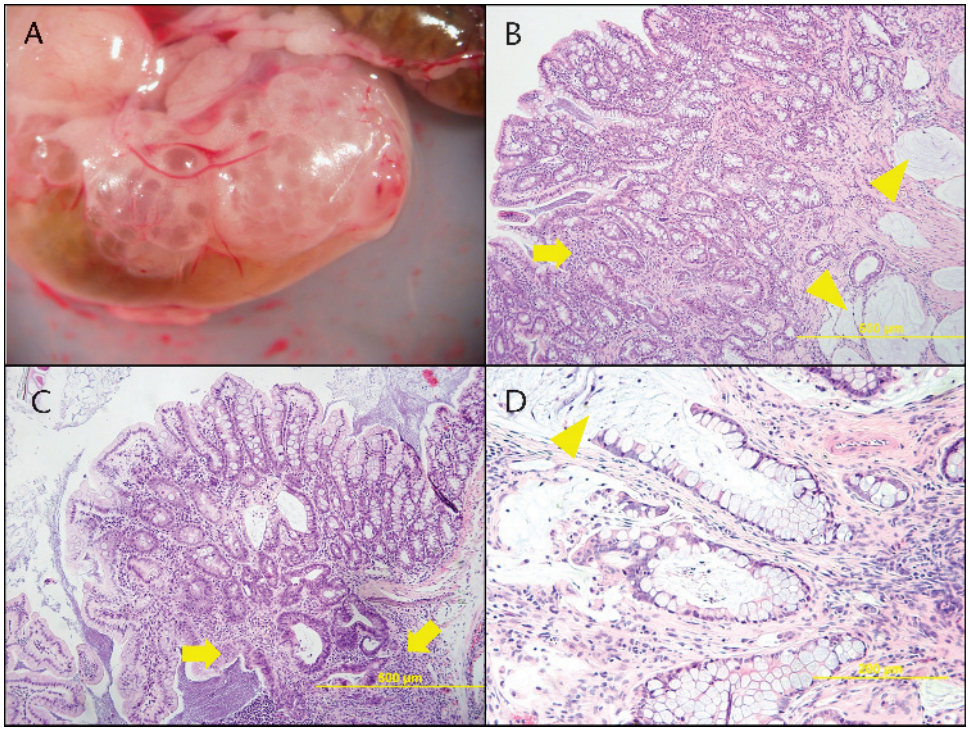

Figure 1. Typical gross (A) and histologic (B-D) appearance of mucinous adenocarcinoma of the proximal colon in *H. bilis*–infected Smad3$^{-/-}$ mice at 9 weeks PI demonstrating the prominent mucin lakes (arrowheads) and tumor-associated inflammatory infiltrates (arrows); images taken at ×100 (B, C) and ×200 (D) of hematoxylin and eosin–stained tissue sections.

Magnetic Resonance Imaging

MRI was performed at 3, 5, 8, 10, 12, 14, and 16 weeks PI using a 7 T/210 mm Varian Unity Inova MRI system equipped with a quadrature-driven birdcage coil (38-mm ID; Varian, Inc, Palo Alto, CA). Mice were anesthetized with 1% to 2% isoflurane in oxygen through a nose cone. A respiratory sensor was placed on the abdomen for monitoring of vital signs; body temperature was supported with warm air circulating in the magnet bore (SA Instruments, Inc, Stony Brook, NY). Coronal and axial planes were collected using a spin-echo T_1-weighted imaging sequence with a fat saturation pulse applied to suppress the strong signals from fatty tissues. Typically, images were collected with 21 slices, 0.8-mm slice thickness, pixel resolution of 59 mm × 127 mm (coronal planes) and 59 mm × 59 mm (axial planes), and four scans to average the motion artifacts. Images were processed using VnmrJ (Varian, Inc, CA).

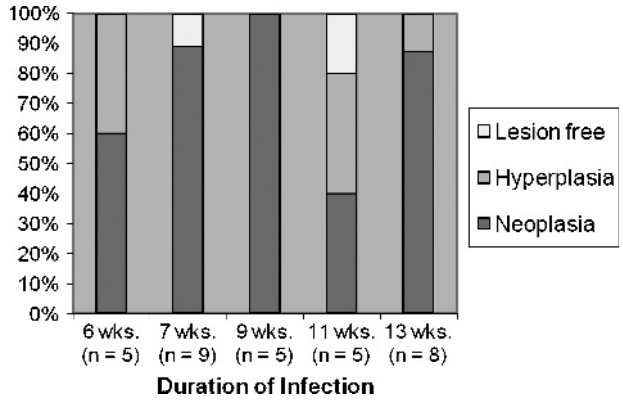

Figure 2. Incidence of neoplasia and hyperplasia in Smad3$^{-/-}$ mice at increasing duration of infection with *H. bilis* as determined by histopathologic analysis.

Sample Collection and Experimental Design

For collection of fecal samples, mice were individually placed in autoclaved cages containing no bedding within a biosafety hood. Fecal pellets were collected at 1, 3, 5, 7, and 9 weeks PI with a sterile tuberculin syringe and placed in 200 µl of RNAlater (Ambion, Austin, TX) for isolation of RNA. Pellets in RNAlater were homogenized with a TissueLyser (Qiagen, Inc, Valencia, CA), centrifuged briefly (Marathon 16 km; Fisher Scientific, Pittsburgh, PA), and then vortexed to resuspend fecal material. After euthanasia, the intestinal tract from ileum to rectum was collected and fixed in formalin.

Histopathology and Ranking of Lesions

Formalin-fixed tissues from *H. bilis*– and sham-infected mice were embedded in paraffin, cut in 5-µm-thick sections, and processed for staining with hematoxylin and eosin. CRC lesions in *H. bilis*–infected mice were ranked in a blinded fashion by two laboratory animal pathologists (A.E. and C.F.) according to lesion severity, based on the number of lesions, the longitudinal and vertical extent of neoplastic lesions, and the degree of associated inflammation. Rankings were compared, and in the case of discrepancies in ranking, pathologists conferred and agreed on a rank order.

RNA Extraction from Feces

Total RNA was extracted using the RNeasy Mini Kit respectively, according to the manufacturer's protocols (Qiagen). RNA was quantified

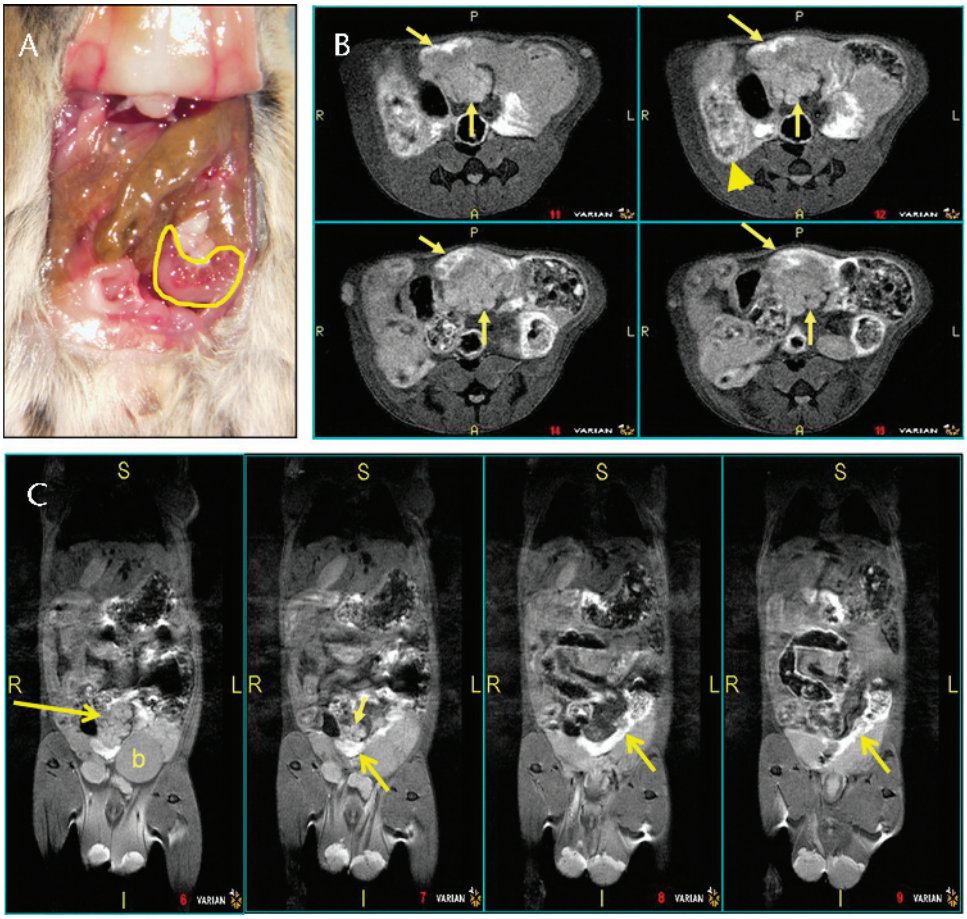

Figure 3. Appearance of mucinous adenocarcinoma *in situ*; outlined (A) and MRI axial images (B) and consecutive micro-MRI coronal images (C) of a male mouse at 16 weeks PI, demonstrating the corresponding lesion (arrows, B, C) and background signal mimicking lesions (arrowhead, B). b indicates bladder.

by measuring the absorbance at 260 and 280 nm using a Nanodrop-1000 spectrophotometer (Nanodrop, Wilmington, DE).

Reverse Transcription

Five micrograms of total RNA was reverse-transcribed using reverse transcriptase and oligo(dT) primers according to the manufacturer's protocol (SuperScript First-Strand; Invitrogen, Carlsbad, CA). cDNA was diluted 1:1 with diethylpyrocarbonate-treated water.

Semiquantitative Real-time Reverse Transcription–Polymerase Chain Reaction

Semiquantitative real-time reverse transcription–polymerase chain reaction (RT-PCR) was used to measure mRNA levels in feces (LightCycler 1.5; Roche Diagnostic, Nutley, NJ). PCRs and melting curves were performed in a 20-μl volume in glass capillaries containing 0.5 μM of each primer, 3 mM $MgCl_2$, QuantiTect SYBR Green PCR Master Mix (Qiagen), and cDNA. To quantify the number of copies of specific cDNA, a standard curve was created using known concentrations (10^1 to 10^6 copies) of the pCR4-TOPO (Invitrogen) plasmid containing the transcript of interest. PCRs were incubated at 95°C for 15 minutes to activate the polymerase followed by 40 cycles consisting of a 15-second denaturing at 94°C, 20-second annealing (see Table 1 for primer-specific annealing temperature), and a 30-second extension at 72°C. The ramp rate was 3°C/sec for annealing and 20°C/sec for all other steps. Fluorescence was monitored at the end of each extension phase. After amplification, melting curves were generated to confirm PCR product identity.

Primer Sequences and Plasmids

The sequences for hypoxanthine guanine phosphoribosyltransferase (HPRT) [18], IL-1β [19], monocyte chemotactic protein 2 (MCP-2) [20], and MIP-1α [21] have been previously reported in the literature. The primer sequence for RANTES was designed from published mRNA sequences using DS Gene software (Accelrys, San Diego, CA). Standards were generated using linearized plasmids containing cloned amplicons of selected targets using the Topo TA PCR cloning kit (Invitrogen). Transcripts were quantified by comparing fluorescence of experimental samples to that of plasmid standards containing known concentrations of the cloned product.

Statistical Analyses

Semiquantitative real-time RT-PCR. Semiquantitative real-time RT-PCR was used to measure mRNA levels in feces. The expressions of IL-1β, MIP-1α, MCP-2, and RANTES were normalized to the expression of the housekeeping gene *HPRT*. The significance of differences in normalized expression levels between *H. bilis*–infected ($n = 7$) and sham-infected ($n = 9$) $Smad3^{-/-}$ mice at 9 weeks PI was determined

using the Mann-Whitney rank sum test. The significance of differences between *H. bilis*–infected MUC+ (n = 11), *H. bilis*–infected MUC– (n = 3), and sham-infected mice (n = 9) at 1 to 7 weeks PI was determined using the Kruskal-Wallis one-way analysis of variance on ranks and Dunn's method of multiple pairwise comparisons.

Correlation to lesion ranks. Coli were evaluated histologically and ranked according to lesion severity. Rank order of lesion severity in *H. bilis*–infected Smad3$^{-/-}$ mice was correlated to the rank order of normalized expression of each biomarker using Spearman rank order correlation (SROC).

Receiver-operator characteristic curves. On the basis of the presence or absence of CRC on histologic interpretation, receiver-operator characteristic (ROC) curves were generated from *H. bilis*–infected (n = 14) Smad3$^{-/-}$ mice using the statistical software package SigmaPlot (SPSS, Chicago, IL). R software [22] was used to compute the confidence intervals (CIs) for the area under the curve (AUC) based on DeLong's method [26] as well as to compare ROC curves to each other based on the Hanley and McNeil method [27]. For CIs for the AUC, upper limits were truncated at unity.

Results

Progression of Colon Cancer in Smad3$^{-/-}$ Mice

Smad3$^{-/-}$ mice on a 129/Sv background develop colonic neoplasia, but this phenotype is dependent on infection with either *H. bilis* or *H. hepaticus*, with tumors developing most often in the proximal colon [11,25]. In the present study, the tumors were typically single masses, although less than 10% developed a second mass at other sites in the colon. Grossly, tumors appeared either as a thickened pale area of the proximal colon or as pearlescent, lobulated, exophytic masses reflecting the abundant mucin production seen in most masses (Figure 1*A*). Histologically, these tumors were best classified as MUC, with an appearance similar to that seen in humans. Tumors were characterized by marked goblet and epithelial cell hyperplasia with extensive production of mucus, often seen sequestered in large dilated "mucin lakes," spilling into the lumen of the gastrointestinal (GI) tract or penetrating the serosal surface and spilling into the peritoneal space. In the latter case, peritonitis was not uncommon. Many of the neoplastic epithelial cells retained a simple tall columnar morphology with centrally located, oblong nuclei containing a vesicular chromatin pattern. There were also abundant goblet cells, often approaching a 1:1 ratio with columnar epithelial cells. Surrounding the accumulations of mucinous material, the epithelium was variably attenuated, and sloughed epithelial and inflammatory cells were seen in the mucinous material, which was characterized by a lightly basophilic, homogenous to lacy appearance (Figure 1, *B-D*). There were also mild to moderate mixed inflammatory infiltrates in the areas around the tumor. Mitotic figures ranged from 0 to 4, with an average of 1 per high-power field (×400). In the absence of *Helicobacter* infection, Smad3$^{-/-}$ mice did not develop MUC or any detectable intestinal inflammation.

Incidence of MUC in Smad3$^{-/-}$ Mice

To determine whether the incidence of MUC would increase with increasing duration of infection, Smad3$^{-/-}$ mice orally infected with *H. bilis*

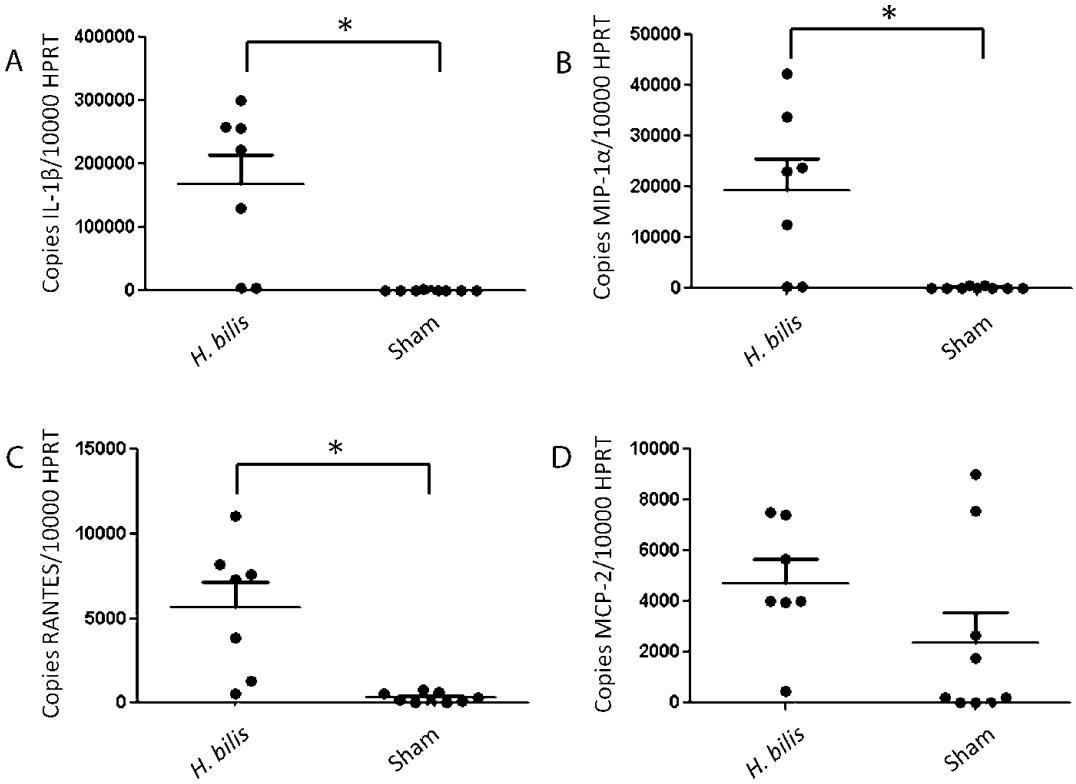

Figure 4. Measurement of IL-1β (A), MIP-1α (B), RANTES (C), and MCP-2 (D) in the feces of Smad3$^{-/-}$ mice at 9 weeks PI as determined by semiquantitative real-time RT-PCR. Data are reported as the mean number of gene transcripts of interest relative to HPRT. Bars, mean and SEM. Statistically significant ($P < .05$) differences between groups are denoted by an asterisk; Mann-Whitney rank sum test.

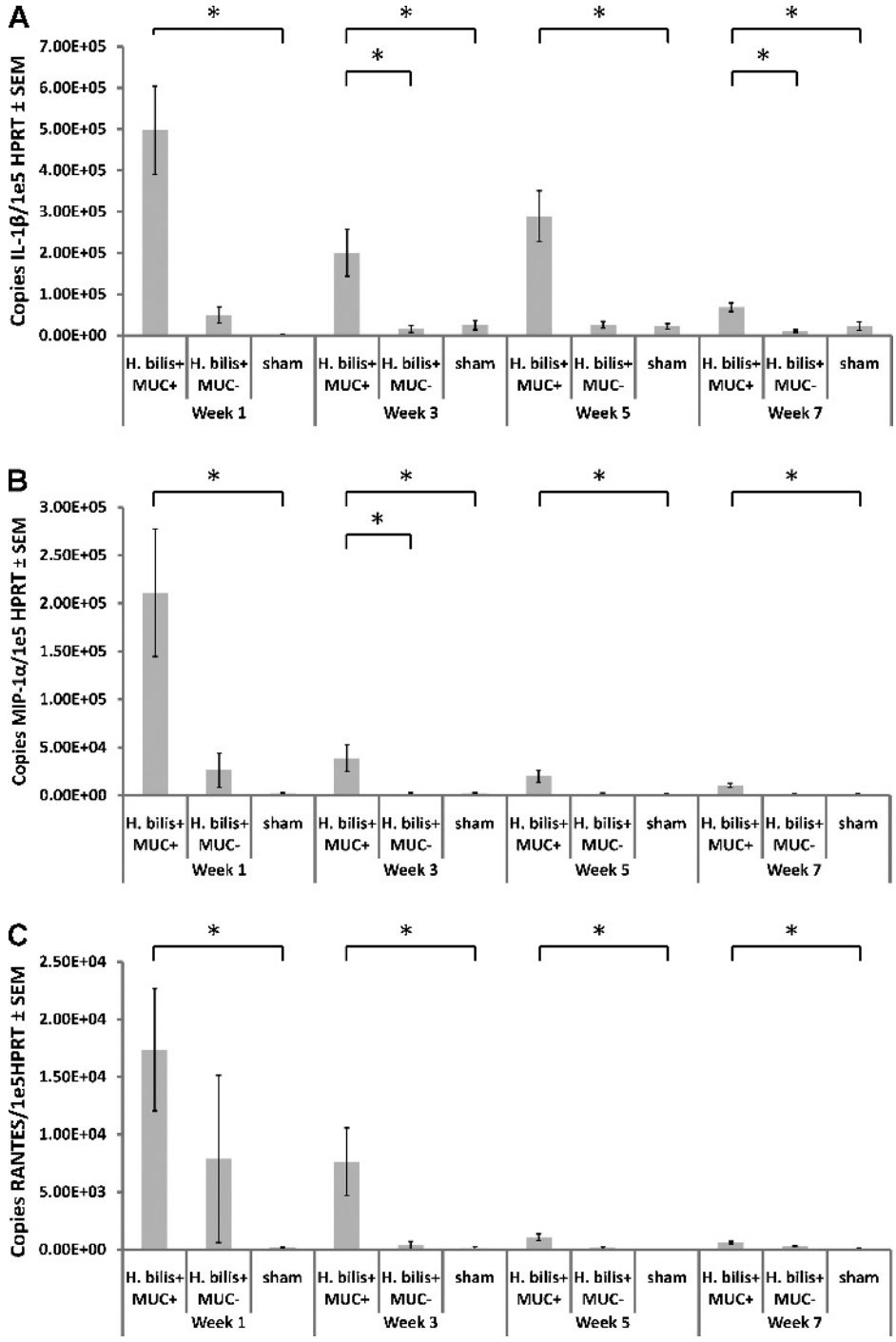

Figure 5. Measurement of IL-1β (A), MIP-1α (B), and RANTES (C) in the feces of Smad3$^{-/-}$ mice from 1 to 7 weeks PI as determined by real-time RT-PCR. Data are reported as the mean number of gene transcripts of interest relative to HPRT. Error bars, SEM. Statistically significant ($P < .05$) differences between groups are denoted by an asterisk; Mann-Whitney rank sum test.

were killed at multiple time points after infection, and the GI tract was collected for histologic examination. Tissues were nominally classified as being neoplastic (possessing a characteristic MUC lesion), hyperplastic (showing evidence of focal or diffuse epithelial hyperplasia but not neoplasia), or lesion-free. Whereas 100% of mice (5/5) examined at 9 weeks PI had developed characteristic MUC lesions, only 40% of mice (2/5) at 11 weeks PI and 88% of mice (7/8) at 13 weeks PI showed histologic evidence of neoplasia (Figure 2). This was not a function of the early time point because similar results were obtained with mice at 20 weeks PI (data not shown). Thus, whereas most mice developed identifiable MUC by as early as 6 weeks PI, not all mice progressed to MUC regardless of the duration of infection.

MRI Detection of MUC in Smad3$^{-/-}$ Mice

H. bilis–infected Smad3$^{-/-}$ mice (n = 12, 6 males and 6 females) and naive wild-type mice of the same background strain (1 male and 1 female) were imaged using MRI without contrast at 3, 5, 8, 10, 12, 14,

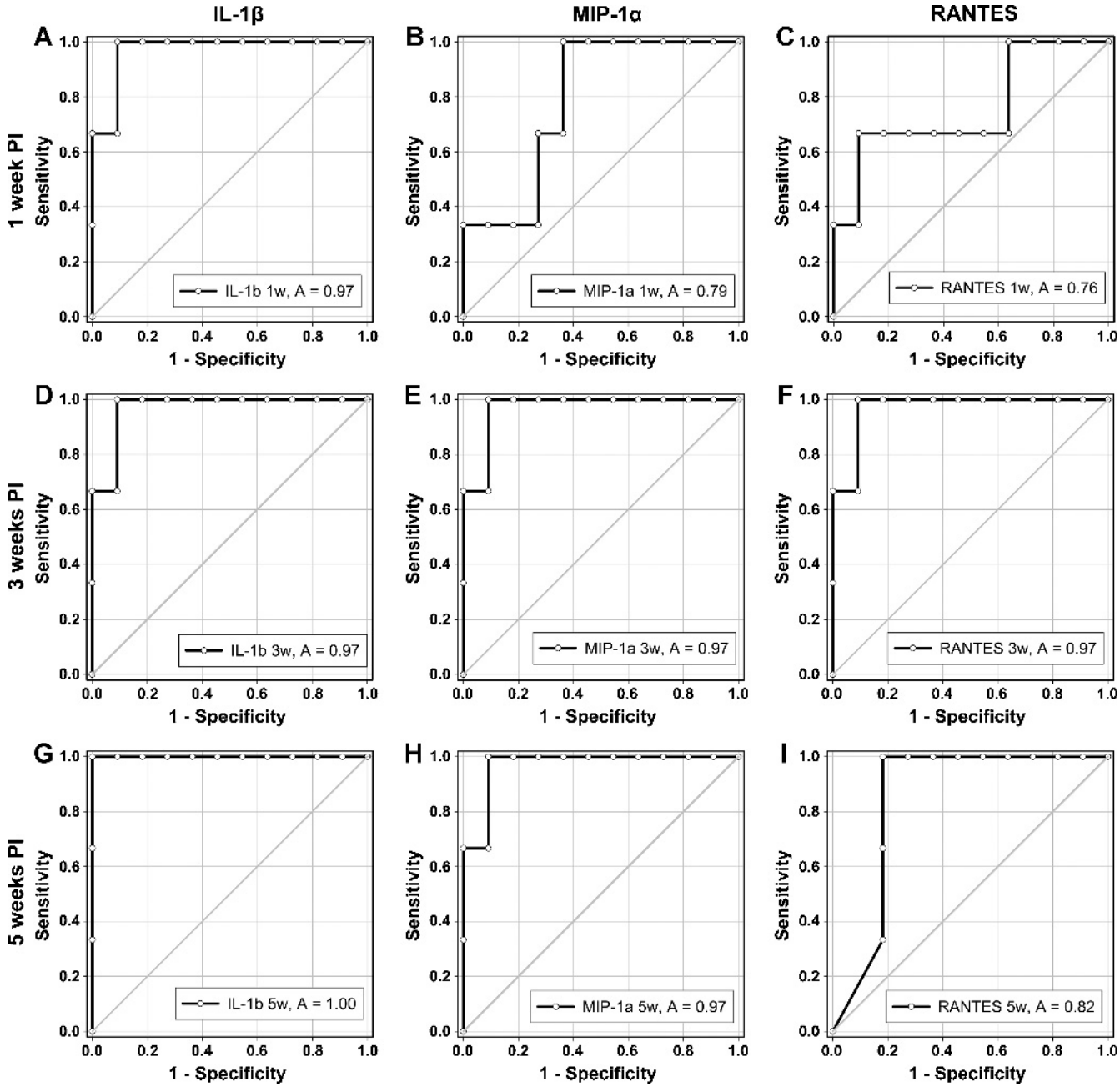

Figure 6. ROC curves for fecal mRNA levels of IL-1β (A, D, G), MIP-1α (B, E, H), and RANTES (C, F, I) at 1 week (A, B, C), 3 weeks (D, E, F), and 5 weeks (G, H, I) PI in the feces of *H. bilis*–infected Smad3$^{-/-}$ mice.

and 16 weeks PI. Immediately after the final imaging, mice were killed and carefully dissected and photographed without disturbing the position of abdominal contents *in situ*. Gross findings were then compared with the 16-week PI images to assess the capacity of MRI to detect intestinal lesions and to evaluate the level of background signal in control mice. The earliest time point at which *Helicobacter*-infected mice were interpreted as possessing a neoplastic lesion was 8 weeks PI. Although we were able to identify a reasonable agreement between

Table 1. Sense and Antisense Primer Pairs Used for Semiquantitative Real-time RT-PCR Amplification.

Gene Name	Sense (5′-3′)	Antisense (3′-5′)	Fragment Size (bp)	Annealing Temperature (°C)
HPRT	GTAATGATCAGTCAACGGGGGAC	CCAGCAAGCTTGCAACCTTAACA	177	60
IL-1β	AGCCCATCCTCTGTGACTCATG	GCTGATGTACCAGTTGGGGAAC	420	57
MCP-2	ACTAAAGCTGAAGATCCCCCTTCG	ACATCACCTGCTTGGTCTGGAAAA	100	57
MIP-1α	GCTCAACATCATGAAGGTCTCC	TGCCGGTTTCTCTTAGTCAGG	222	57
RANTES	GAGTATTTCTACACCAGCAGC	GGACTAGAGCAAGCAATGC	192	60

the final (16 weeks PI) images and gross necropsy findings in 7 of 12 *H. bilis*–infected mice (sensitivity = 58.33%; Figure 3), 5 of 12 mice with histologically identifiable MUC were interpreted as MUC-negative at 16 weeks PI.

Fecal Cytokine Gene Expression as a Biomarker of MUC at 9 Weeks PI in H. bilis*–Infected Smad3$^{-/-}$ Mice*

At 9 weeks PI, *H. bilis*–infected Smad3$^{-/-}$ mice expressed significantly higher levels of IL-1β ($P = .001$, Mann-Whitney rank sum test), MIP-1α ($P = .004$), and RANTES ($P = .003$; Figure 4, *A-C*). However, no difference was detected in the expression of MCP-2 despite a trend toward an elevated expression in *H. bilis*–infected mice (Figure 4*D*). Two sham-inoculated mice expressed levels of MCP-2 comparable to even the highest-expressing *H. bilis*–infected mice; thus, MCP-2 was eliminated from further experiments. In this cohort of mice, all seven *Helicobacter*-infected mice developed histologically identifiable MUC. SROC was then performed to correlate the expression of IL-1β, MIP-1α, and RANTES with lesion severity in the *H. bilis*–infected mice. Correlation coefficients for IL-1β, MIP-1α, and RANTES were 0.929 ($P < .001$), 0.536 ($P = .18$), and 0.750 ($P = .04$), respectively, indicating a significant correlation between lesion scores and expression of both IL-1β and RANTES. On the basis of the significant overall difference in expression between infected and control mice in MIP-1α expression, along with the fact that the two mice with the lowest MIP-1α mRNA levels also demonstrated the lowest lesion scores, we opted to retain MIP-1α in subsequent studies. In addition, the kinetics of chemokine and cytokine expression vary, and we reasoned that, at earlier time points, MIP-1α might still prove to be a useful biomarker, despite poor overall correlation at 9 weeks PI.

Fecal Cytokine Gene Expression during the Progression of MUC in H. bilis*–Infected Smad3$^{-/-}$ Mice*

To determine whether fecal mRNA levels of IL-1β, MIP-1α, and RANTES at time points earlier than 9 weeks PI could predict subsequent disease occurrence or severity, mice were inoculated as before with *H. bilis* ($n = 14$) or sterile broth ($n = 9$), and fecal samples were collected every 2 weeks starting at 1 week PI and continuing until 7 weeks PI. Mice were killed at 9 weeks PI, and tissues were collected for histologic examination. The normalized expression of each biomarker was determined at each time point, revealing similar kinetics for all three biomarkers (Figure 5). The expression of all three biomarkers peaked at 1 week PI and then steadily declined thereafter in *Helicobacter*-infected mice. Nonetheless, even at 7 weeks PI, there was a significant difference (Mann-Whitney rank sum test, $P < .05$) between *H. bilis*–infected MUC+ and sham-infected mice for all three biomarkers.

To assess the value of each biomarker and determine the optimal screening paradigm, the expression at each time point was correlated to lesion rank at 9 weeks PI using SROC. In addition, ROC curves were generated to establish sensitivity, specificity, and appropriate cutoff values for each biomarker. SROC analysis of samples from 1 to 7 weeks PI revealed a significant correlation ($P < .05$) between lesion severity at 9 weeks PI and expression of IL-1β at 1, 3, and 5 weeks PI, of MIP-1α at 3 and 5 weeks PI, and of RANTES at 3 weeks PI, indicating that 3 weeks PI may be the optimal time for testing mice. Surprisingly, the correlation between lesion rank and the expression of all three biomarkers was not statistically significant at 7 weeks PI. However, SROC indicates the overall agreement between lesions and the selected biomarkers across the entire range of lesion severity. Because our goal was to identify "poor responders" and eliminate mice at the low end of the disease spectrum, ROC curves at each time point were compared with determine whether very high specificity (>0.98) and acceptable sensitivity (>0.80) could be achieved simultaneously. Considering the poor correlation for all markers at 7 weeks PI, empirical ROC curves were produced for only 1, 3, and 5 weeks PI (Figure 6). CIs were established using the method of DeLong et al. [26], and the upper limit was truncated at 1 because AUC values, by definition, cannot exceed unity. All three biomarkers examined provided an estimated AUC of 0.97 at 3 weeks PI (Figure 6, *D-F*; 95% CI = 0.89-1). At 5 weeks PI, however, fecal mRNA levels of IL-1β yielded an estimated AUC of 1, thus providing, in this sample, perfect sensitivity and specificity in predicting the presence or absence of MUC in mice at 9 weeks PI (Figure 6*G*). However, ranking the relative performance of IL-1β at 5 weeks PI and IL-1β, MIP-1α, or RANTES at 3 weeks PI is difficult because the small sample size gives limited power to discern differences in AUC; not surprisingly, none of the markers shown in Figure 6 were statistically different from each other (smallest $P = .1$), using the method of Hanley and McNeil [27]. Because the goal of this study was to establish a screening method with the ability to predict which mice would not develop CRC as a means of conserving resources, it should be noted that by as early as 1 week PI, IL-1β provided an AUC of 0.97 (95% CI = 0.89-1), the same as all three biomarkers at 3 weeks PI. In addition, the overall correlation between lesion severity rank at 9 weeks PI and fecal mRNA levels of IL-1β at 1 week PI was 0.65 ($P = .01$; SROC). Thus, we propose that in this model of MUC, RT-PCR analysis of fecal mRNA specific for IL-1β at 1 week PI or of IL-1β, MIP-1α, or RANTES at 3 weeks PI is a reliable, noninvasive determinant of which mice will not progress to MUC. More importantly, this provides a proof of principle that fecal nucleic acid analysis has utility in mouse models of gastrointestinal neoplasia, as a means of reducing the number of animals used in study. This may also portend novel screening methods of interest to the human population.

Discussion

The World Health Organization defines MUC in humans as a tumor with more than 50% showing a mucinous pattern on histologic examination and with a large amount of extracellular mucin produced by secreting acini [28]. Of CRC, MUC accounts for between 11% and 15% [29]. *Helicobacter*-infected Smad3$^{-/-}$ mice recapitulate the human condition faithfully, with extensive mucin production seen multifocally in neoplastic foci, forming dilated pockets of mucinous material extending into the lumen and frequently through the tunica muscularis to the serosal surface of the GI tract. There are several reasons to believe that the mechanisms leading to MUC in humans and *Helicobacter*-infected Smad3$^{-/-}$ mice are similar. In humans, as in *Helicobacter*-infected Smad3$^{-/-}$ mice, MUC occurs more frequently in the proximal colon than elsewhere in the GI tract [30–32]. Although not all studies agree, possibly due to geographical differences [33] or the presence of two subtypes of colorectal MUC [30], MUC in humans seems to be more prevalent as a sequela to IBD than as a spontaneous CRC not associated with previous IBD [32,34–37]. Supporting this concept, MUC occurs primarily in areas of chronic inflammation, and the risk of MUC increases with duration of IBD [38,39]. Similarly, the findings detailed herein support the notion that the severity of MUC in *Helicobacter*-infected Smad3$^{-/-}$ mice is largely dependent on the robustness of the inflammatory response to a member of the gut flora, as measured by the expression of certain fecal cytokines and chemokines. In addition, MUC in humans is frequently associated with fistula formation

[32,35,40–43], a phenomenon attributed to adenomatous transformation of the epithelium lining the fistula tract [44]. Many *H. bilis*–infected Smad3$^{-/-}$ mice showed histologic evidence of perforation of the bowel wall and areas in which dysplastic epithelial cells are seen invading and penetrating the serosal surface (Figure 1, *B-D*), and it is tempting to speculate that a similar mechanism is at work in the formation of MUC lesions in Smad3$^{-/-}$ mice.

Regardless of the pathogenesis, not all Smad3$^{-/-}$ mice will develop MUC despite persistent colonization with *H. bilis*. As a consequence, many of these MUC-resistant mice will be used in expensive therapeutic trials lasting up to 8 months in duration. Along with the time and money spent maintaining mice that will not progress to MUC, one must also consider that these mice are potentially confounding the research by making therapeutic compounds seem falsely efficacious. The ability to noninvasively identify which mice will not progress to cancer would both conserve resources and increase the power of data generated by using only mice with a high probability of developing MUC. We first evaluated MRI as a means of detecting early inflammatory or precancerous lesions in *Helicobacter*-infected Smad3$^{-/-}$ mice. Mice were imaged every 2 to 3 weeks until 16 weeks PI, a time by which previous studies (Figure 2) had demonstrated most mice would develop MUC. Although MRI provided some diagnostic information, that is, the presence or absence of a lesion, it afforded little prognostic information regarding the severity or extent of disease at necropsy when images were analyzed retrospectively. This is partially due to the variability between images from week to week. Frequently, MRI would indicate a possible lesion at one time point, followed by images at subsequent time points interpreted as negative. In only 1 of 12 mice did images consistently contain suspect lesions after the initial appearance. In addition, in those mice in which a correlation between 16-week PI MRI images and gross lesions was detected, it was difficult to reliably track the course of intestinal neoplasms retrospectively. The background noise, seen in both experimental and control mice, was considerable and was most problematic in highly glandular tissue such as the reproductive tract. In addition, the severity of the lesions could not be predicted based on the size and intensity of suspect lesions on MRI. Mice with hyperintense signal on the final imaging, indicating a large or severe lesion, often revealed mild or moderate MUC lesions at necropsy. Conversely, mice with borderline "positive" final images often revealed extensive marked MUC or even multiple lesions. MRI has been applied to the human population as a screening method for MUC; however, the method requires insufflation of the colon with air to enhance imaging [1]. The lack of insufflation in our study may partially explain the lack of adequate definition with MRI. Also, the imaging in this study was performed without the use of contrast. MRI studies of the gastrointestinal tract using a fecal-tagging based MRI contrast agent may enhance visualization of MUC lesions [45]. The primary goal of these studies was to evaluate two distinct methods of detecting CRC in a mouse model, noninvasively and as early in the disease process as possible. Because our motivation was to conserve resources, we opted to omit insufflation and contrast in an effort to keep the procedure as simple and cost-effective as possible. In our study, a mass showing hyperintense and heterogeneous signal contents would indicate a MUC lesion (Figure 3, *B* and *C*). However, abdominal motion artifacts and significant signals from feces often cause ambiguities or missed detections. A respiratory-gated T_2-weighted MRI protocol may be applied to increase the detection accuracy and specificity for MUC because of the brighter signal nature of mucin contents in MUC lesions on T_2-weighted images, however, with the expense of prolonged imaging time. Lastly, considering the expense of the initial purchase, maintenance, and operation, MRI is a costly technique for screening large numbers of animals. Imaging in both coronal and axial planes resulted in 21 and 42 images, respectively, per mouse at each time point, which, along with the user-dependent nature of image interpretation, made this a time-consuming and subjective technique. Because our impetus for screening animals is to eliminate mice that are not going to develop MUC as a means of saving costs, MRI is problematic. Thus, the inability of MRI to detect disease in a reproducible manner, the associated costs, and the labor-intensive and subjective nature of this method make it less than ideal for our purposes.

Next, we elected to determine whether CRC in our model could be predicted through the analysis of fecal cytokine and chemokine message levels. This concept, although not new in humans [46,47], has not been applied to murine models to the authors' knowledge. Because humans and mice both constitutively slough colonic epithelial cells in feces, the RNA isolated from these cells should reflect the state of health or inflammation present in the gut. Inflammation is now recognized as a risk factor and negative prognostic indicator for certain types of neoplasia in humans [48]. Adaptive antitumoral immune responses, particularly those mediated by CD8$^+$ T cells, are considered protective and beneficial in destroying tumor cells, whereas inflammation due to innate immune responses is often associated with a poor prognosis [49]. This concept can be extrapolated to the chemokines responsible for attracting T cells or macrophages; accumulation of lymphocytes due to increased expression of CXCL16 correlates with a favorable outcome in human CRC [50], whereas accumulation of tumor-associated macrophages due to increased levels of CCL2 correlates with poor outcome [51]. Thus, as a means of noninvasively assessing the degree of colonic inflammation in Smad3$^{-/-}$ mice, we measured the fecal levels of several factors involved in macrophage recruitment, and which have been shown to be elevated in human CRC [49,52,53], including the chemokines MIP-1α, RANTES, and MCP-2 and IL-1β, a highly pleiotropic proinflammatory cytokine with effects on virtually all cell types [54]. Our initial fecal biomarker study was performed at 9 weeks PI, when most mice were expected to have developed MUC. It was established that a significant difference in the fecal expression of IL-1β, MIP-1α, and RANTES existed between *Helicobacter*- and sham-infected mice (Figure 4); however, 100% (7/7) of the infected mice in this group developed MUC, making a comparison of MUC+ and MUC– mice within the infected group impossible. Pursuing earlier time points PI (Figure 5) with a second group of mice provided evidence that there is also a significant difference in the expression of these biomarkers between *H. bilis*–infected MUC+ and MUC– mice, supporting their use as predictors of MUC in this model. It is notable that the expression of IL-1β, MIP-1α, and RANTES showed an acute increase after infection with *Helicobacter*, which waned steadily thereafter. Although these biomarkers are primarily associated with innate immune responses, infection with *H. bilis* eventually induces an adaptive immune response [55], allowing the innate response to wane accordingly. Like the selected chemokines, IL-1β is produced by the intestinal epithelium. Because intestinal epithelial cells also express the activating receptor IL-1RI [54], IL-1β functions in an autocrine and paracrine manner to amplify chemokine expression. Similarly, RANTES has been shown to stimulate production of MIP-1α by human monocytes [56], suggesting that activation of tumor-associated macrophages may amplify recruitment of additional monocytes and other leukocytes, thought to be the source of harmful reactive oxidative intermediaries. Interestingly, several studies indicate

that IL-1β may have a more direct role in colorectal tumorigenesis. In 2003, Liu et al. [57] demonstrated that IL-1β upregulates the expression of cyclooxygenase-2 (COX-2), which is overexpressed in 80% to 90% of human CRC [58] and is also found to be elevated in *Helicobacter*-infected Smad3 sup>–/– mice relative to naive mice [11]. Similarly, Maihofner et al. [59] showed that, in both human CRC-associated neoplastic epithelium and tumor-associated macrophages, COX-2 expression was markedly increased and that increase correlated with increases in IL-1β. COX-2 functions to facilitate tumor development through the induction of antiapoptotic and angiogenic factors [60,61], and it is worth noting that fecal mRNA levels of COX-2 have been evaluated as screening techniques for human CRC [62,63]. In addition, IL-1β has a potent proliferative effect on human carcinoma cell lines [64], most likely through the induction of other growth factors. With regard to the mucinous phenotype seen in *Helicobacter*-infected Smad3$^{-/-}$ mice, IL-1β has been shown to upregulate the expression and release of mucins in both colonic epithelial cell lines [65,66] and perfused rat colon [67]. Regardless of the mechanism, the present data suggest that MUC in Smad3$^{-/-}$ mice is highly correlated with the previous expression of IL-1β, MIP-1α, and RANTES.

Until recently, the amplification of nucleic acids from feces has been hindered by poor recovery because of the presence of nucleases. DNA is much more stable than RNA and can typically be amplified from feces that have been snap-frozen in liquid nitrogen. However, because of the inherent instability of RNA and the abundance of prokaryotic nucleases in the feces, a preservative containing RNAse inhibitors is needed to isolate mRNA from feces. When compared with several other methods of RNA preservation including liquid nitrogen, silica gel, Whatman FTA cards, and Paxgene, Yu et al. [68] found RNAlater to provide the optimal quantity and quality of RNA as well as the lowest level of genomic DNA contamination. For our studies, two fecal pellets per mouse were collected in 200 μl of RNAlater at each time point, yielding 600 to 800 ng/μl RNA per sample. Assuming an average mass of 35 mg per fecal pellet, this results in an average yield of approximately 70 μg of RNA per gram of feces. An early description of a similar technique applied to human stool yielded from 5 to 30 μg of RNA per gram of stool from CRC patients and approximately 5 μg of RNA per gram from healthy controls [46]. Several points should be made regarding this difference. An obvious caveat is the different methods of RNA extraction from feces. Although the present data represent RNA extracted using a commercially available kit from feces preserved in RNAlater, the samples from human CRC patients and controls were snap-frozen in liquid nitrogen, and RNA was extracted with acid phenol and chloroform. A second consideration regarding differences in RNA recovery from mouse and human stool is the fate of senescent epithelial colonocytes. In humans, effete colonocytes are primarily removed through mucosal phagocytosis, allowing subcellular components to be recycled [69]. Alternatively, colonocytes in rodents are lost primarily through simple exfoliation into the lumen [69]. Thus, it would be expected that rodent feces would contain more RNA on a per-weight basis and may be ideally suited to molecular techniques such as those described here.

There is a strong likelihood that these techniques are applicable to other mouse models of CRC. One would expect that postinflammatory models of intestinal neoplasia would be particularly amenable to fecal cytokine or chemokine analysis. Several other strains of mice used as models of colitis are also prone to CRC, including IL-10$^{-/-}$ mice [70], IL-2^{null} × β2m^{null} mice [71], and $G_{\alpha i2}{}^{-/-}$ mice [72] among others. In each model, while the development of colitis precedes CRC, suggesting that CRC is driven by the inflammatory response, only 31% to 60% of mice in these models will progress to carcinoma [37]. Thus, while the appropriate biomarkers and their kinetics would need to be established for each model (and possibly laboratory), the concept of predicting the presence or severity of disease using fecal biomarkers of inflammation likely applies to more than just the Smad3$^{-/-}$ mouse model. Similarly, several fecal biomarkers, including RNA specific for COX-2 and matrix metalloproteinase 7, have garnered interest as screening tools for CRC in humans [62,63]. As microarray technologies become more commonplace, the use of fecal RNA analysis may allow for robust, noninvasive CRC screening in humans. Smad3$^{-/-}$ mice offer a useful tool for these types of studies, and the refinement of the model described herein will enhance the development of both screening techniques and therapeutic modalities for CRC.

Acknowledgments

The authors thank the Department of Veterans Affairs for use of facilities and resources at the Harry S. Truman Memorial Veterans' Hospital in Columbia, MO.

References

[1] Walsh JM and Terdiman JP (2003). Colorectal cancer screening: scientific review. *JAMA* **289**, 1288–1296.
[2] Itzkowitz SH (2006). Molecular biology of dysplasia and cancer in inflammatory bowel disease. *Gastroenterol Clin North Am* **35**, 553–571.
[3] Dukes CE (1932). The classification of cancer of the rectum. *J Pathol Bacteriol* **35**, 323.
[4] Astler VB and Coller FA (1954). The prognostic significance of direct extension of carcinoma of the colon and rectum. *Ann Surg* **139**, 846–852.
[5] Ouyang DL, Chen JJ, Getzenberg RH, and Schoen RE (2005). Noninvasive testing for colorectal cancer: a review. *Am J Gastroenterol* **100**, 1393–1403.
[6] Burch JA, Soares-Weiser K, St John DJ, Duffy S, Smith S, Kleijnen J, and Westwood M (2007). Diagnostic accuracy of faecal occult blood tests used in screening for colorectal cancer: a systematic review. *J Med Screen* **14**, 132–137.
[7] Doria-Rose VP, Newcomb PA, and Levin TR (2005). Incomplete screening flexible sigmoidoscopy associated with female sex, age, and increased risk of colorectal cancer. *Gut* **54**, 1273–1278.
[8] Huang EH, Carter JJ, Whelan RL, Liu YH, Rosenberg JO, Rotterdam H, Schmidt AM, Stern DM, and Forde KA (2002). Colonoscopy in mice. *Surg Endosc* **16**, 22–24.
[9] Becker C, Fantini MC, and Neurath MF (2006). High resolution colonoscopy in live mice. *Nat Protoc* **1**, 2900–2904.
[10] Datto MB, Frederick JP, Pan L, Borton AJ, Zhuang Y, and Wang XF (1999). Targeted disruption of Smad3 reveals an essential role in transforming growth factor β–mediated signal transduction. *Mol Cell Biol* **19**, 2495–2504.
[11] Maggio-Price L, Treuting P, Zeng W, Tsang M, Bielefeldt-Ohmann H, and Iritani BM (2006). *Helicobacter* infection is required for inflammation and colon cancer in SMAD3-deficient mice. *Cancer Res* **66**, 828–838.
[12] Fox JG, Yan L, Shames B, Campbell J, Murphy JC, and Li X (1996). Persistent hepatitis and enterocolitis in germfree mice infected with *Helicobacter hepaticus*. *Infect Immun* **64**, 3673–3681.
[13] Myles MH, Livingston RS, Livingston BA, Criley JM, and Franklin CL (2003). Analysis of gene expression in ceca of *Helicobacter hepaticus*–infected A/JCr mice before and after development of typhlitis. *Infect Immun* **71**, 3885–3893.
[14] Grady WM, Rajput A, Myeroff L, Liu DF, Kwon K, Willis J, and Markowitz S (1998). Mutation of the type II transforming growth factor-β receptor is coincident with the transformation of human colon adenomas to malignant carcinomas. *Cancer Res* **58**, 3101–3104.
[15] Markowitz SD and Bertagnolli MM (2009). Molecular origins of cancer: molecular basis of colorectal cancer. *N Engl J Med* **361**, 2449–2460.
[16] Livingston RS, Riley LK, Steffen EK, Besch-Williford CL, Hook RR Jr, and Franklin CL (1997). Serodiagnosis of *Helicobacter hepaticus* infection in mice by an enzyme-linked immunosorbent assay. *J Clin Microbiol* **35**, 1236–1238.
[17] Riley LK, Franklin CL, Hook RR Jr, and Besch-Williford C (1996). Identification of murine helicobacters by PCR and restriction enzyme analyses. *J Clin Microbiol* **34**, 942–946.

[18] O'Garra A, Chang R, Go N, Hastings R, Haughton G, and Howard M (1992). Ly-1 B (B-1) cells are the main source of B cell–derived interleukin 10. *Eur J Immunol* **22**, 711–717.

[19] Kruessel JS, Huang HY, Wen Y, Kloodt AR, Bielfeld P, and Polan ML (1997). Different pattern of interleukin-1 β– (IL-1 β), interleukin-1 receptor antagonist-(IL-1ra) and interleukin-1 receptor type I– (IL-1R tI) mRNA-expression in single preimplantation mouse embryos at various developmental stages. *J Reprod Immunol* **34**, 103–120.

[20] Huang DR, Wang J, Kivisakk P, Rollins BJ, and Ransohoff RM (2001). Absence of monocyte chemoattractant protein 1 in mice leads to decreased local macrophage recruitment and antigen-specific T helper cell type 1 immune response in experimental autoimmune encephalomyelitis. *J Exp Med* **193**, 713–726.

[21] Myles MH, Dieckgraefe BK, Criley JM, and Franklin CL (2007). Characterization of cecal gene expression in a differentially susceptible mouse model of bacterial-induced inflammatory bowel disease. *Inflamm Bowel Dis* **13**, 822–836.

[22] Team RDC (2010). *R: A Language and Environment for Statistical Computing*.

[23] Brasil P (2010). *DiagnosisMed: Diagnostic Test Accuracy Evaluation for Medical Professionals*.

[24] Vinterbo SA (2007). *gcl: Compute a Fuzzy Rules or Tree Classifier from Data*.

[25] Zhu Y, Richardson JA, Parada LF, and Graff JM (1998). Smad3 mutant mice develop metastatic colorectal cancer. *Cell* **94**, 703–714.

[26] DeLong ER, DeLong DM, and Clarke-Pearson DL (1988). Comparing the areas under two or more correlated receiver operating characteristic curves: a nonparametric approach. *Biometrics* **44**, 837–845.

[27] Hanley JA and McNeil BJ (1983). A method of comparing the areas under receiver operating characteristic curves derived from the same cases. *Radiology* **148**, 839–843.

[28] Symonds DA and Vickery AL (1976). Mucinous carcinoma of the colon and rectum. *Cancer* **37**, 1891–1900.

[29] Kakar S, Aksoy S, Burgart LJ, and Smyrk TC (2004). Mucinous carcinoma of the colon: correlation of loss of mismatch repair enzymes with clinicopathologic features and survival. *Mod Pathol* **17**, 696–700.

[30] Leopoldo S, Lorena B, Cinzia A, Gabriella DC, Angela Luciana B, Renato C, Antonio M, Carlo S, Cristina P, Stefano C, et al. (2008). Two subtypes of mucinous adenocarcinoma of the colorectum: clinicopathological and genetic features. *Ann Surg Oncol* **15**, 1429–1439.

[31] Halvorsen TB and Seim E (1988). Influence of mucinous components on survival in colorectal adenocarcinomas: a multivariate analysis. *J Clin Pathol* **41**, 1068–1072.

[32] Wyatt MG, Houghton PW, Mortensen NJ, and Williamson RC (1987). The malignant potential of colorectal Crohn's disease. *Ann R Coll Surg Engl* **69**, 196–198.

[33] Levin KE and Dozois RR (1991). Epidemiology of large bowel cancer. *World J Surg* **15**, 562–567.

[34] Rubio CA and Befrits R (1997). Colorectal adenocarcinoma in Crohn's disease: a retrospective histologic study. *Dis Colon Rectum* **40**, 1072–1078.

[35] Winkler R, Wittmer A, and Heusermann U (2002). Cancer and Crohn's disease. *Z Gastroenterol* **40**, 569–576.

[36] Hamilton SR (1985). Colorectal carcinoma in patients with Crohn's disease. *Gastroenterology* **89**, 398–407.

[37] Itzkowitz SH and Yio X (2004). Inflammation and cancer: IV. Colorectal cancer in inflammatory bowel disease: the role of inflammation. *Am J Physiol Gastrointest Liver Physiol* **287**, G7–G17.

[38] Choi PM and Zelig MP (1994). Similarity of colorectal cancer in Crohn's disease and ulcerative colitis: implications for carcinogenesis and prevention. *Gut* **35**, 950–954.

[39] Weedon DD, Shorter RG, Ilstrup DM, Huizenga KA, and Taylor WF (1973). Crohn's disease and cancer. *N Engl J Med* **289**, 1099–1103.

[40] Ky A, Sohn N, Weinstein MA, and Korelitz BI (1998). Carcinoma arising in anorectal fistulas of Crohn's disease. *Dis Colon Rectum* **41**, 992–996.

[41] Moore-Maxwell CA and Robboy SJ (2004). Mucinous adenocarcinoma arising in rectovaginal fistulas associated with Crohn's disease. *Gynecol Oncol* **93**, 266–268.

[42] Ying LT, Hurlbut DJ, Depew WT, Boag AH, and Taguchi K (1998). Primary adenocarcinoma in an enterocutaneous fistula associated with Crohn's disease. *Can J Gastroenterol* **12**, 265–269.

[43] Kudo K, Funayama Y, Fukushima K, Shibata C, Takahashi K, Ogawa H, Ueno T, Haneda S, Watanabe K, Koyama A, et al. (2007). Carcinoma arising from ileorectal fistula in a patient with Crohn's disease. *Nippon Shokakibyo Gakkai Zasshi* **104**, 1492–1497.

[44] Smith R, Hicks D, Tomljanovich PI, Lele SB, Rajput A, and Dunn KB (2008). Adenocarcinoma arising from chronic perianal Crohn's disease: case report and review of the literature. *Am Surg* **74**, 59–61.

[45] Kuehle CA, Langhorst J, Ladd SC, Zoepf T, Nuefer M, Grabellus F, Barkhausen J, Gerken G, and Lauenstein TC (2007). Magnetic resonance colonography without bowel cleansing: a prospective cross sectional study in a screening population. *Gut* **56**, 1079–1085.

[46] Alexander RJ and Raicht RF (1998). Purification of total RNA from human stool samples. *Dig Dis Sci* **43**, 2652–2658.

[47] Hasegawa Y, Takeda S, Ichii S, Koizumi K, Maruyama M, Fujii A, Ohta H, Nakajima T, Okuda M, Baba S, et al. (1995). Detection of K-*ras* mutations in DNAs isolated from feces of patients with colorectal tumors by mutant-allele–specific amplification (MASA). *Oncogene* **10**, 1441–1445.

[48] Il'yasova D, Colbert LH, Harris TB, Newman AB, Bauer DC, Satterfield S, and Kritchevsky SB (2005). Circulating levels of inflammatory markers and cancer risk in the health aging and body composition cohort. *Cancer Epidemiol Biomarkers Prev* **14**, 2413–2418.

[49] Erreni M, Bianchi P, Laghi L, Mirolo M, Fabbri M, Locati M, Mantovani A, and Allavena P (2009). Expression of chemokines and chemokine receptors in human colon cancer. *Methods Enzymol* **460**, 105–121.

[50] Hojo S, Koizumi K, Tsuneyama K, Arita Y, Cui Z, Shinohara K, Minami T, Hashimoto I, Nakayama T, Sakurai H, et al. (2007). High-level expression of chemokine CXCL16 by tumor cells correlates with a good prognosis and increased tumor-infiltrating lymphocytes in colorectal cancer. *Cancer Res* **67**, 4725–4731.

[51] Bailey C, Negus R, Morris A, Ziprin P, Goldin R, Allavena P, Peck D, and Darzi A (2007). Chemokine expression is associated with the accumulation of tumour associated macrophages (TAMs) and progression in human colorectal cancer. *Clin Exp Metastasis* **24**, 121–130.

[52] Lewis CE and Pollard JW (2006). Distinct role of macrophages in different tumor microenvironments. *Cancer Res* **66**, 605–612.

[53] Baier PK, Eggstein S, Wolff-Vorbeck G, Baumgartner U, and Hopt UT (2005). Chemokines in human colorectal carcinoma. *Anticancer Res* **25**, 3581–3584.

[54] Dinarello CA (1996). Biologic basis for interleukin-1 in disease. *Blood* **87**, 2095–2147.

[55] Jergens AE, Wilson-Welder JH, Dorn A, Henderson A, Liu Z, Evans RB, Hostetter J, and Wannemuehler MJ (2007). *Helicobacter bilis* triggers persistent immune reactivity to antigens derived from the commensal bacteria in gnotobiotic C3H/HeN mice. *Gut* **56**, 934–940.

[56] Locati M, Deuschle U, Massardi ML, Martinez FO, Sironi M, Sozzani S, Bartfai T, and Mantovani A (2002). Analysis of the gene expression profile activated by the CC chemokine ligand 5/RANTES and by lipopolysaccharide in human monocytes. *J Immunol* **168**, 3557–3562.

[57] Liu W, Reinmuth N, Stoeltzing O, Parikh AA, Tellez C, Williams S, Jung YD, Fan F, Takeda A, Akagi M, et al. (2003). Cyclooxygenase-2 is up-regulated by interleukin-1β in human colorectal cancer cells via multiple signaling pathways. *Cancer Res* **63**, 3632–3636.

[58] Sano H, Kawahito Y, Wilder RL, Hashiramoto A, Mukai S, Asai K, Kimura S, Kato H, Kondo M, and Hla T (1995). Expression of cyclooxygenase-1 and -2 in human colorectal cancer. *Cancer Res* **55**, 3785–3789.

[59] Maihofner C, Charalambous MP, Bhambra U, Lightfoot T, Geisslinger G, and Gooderham NJ (2003). Expression of cyclooxygenase-2 parallels expression of interleukin-1β, interleukin-6 and NF-κB in human colorectal cancer. *Carcinogenesis* **24**, 665–671.

[60] Tsujii M and DuBois RN (1995). Alterations in cellular adhesion and apoptosis in epithelial cells overexpressing prostaglandin endoperoxide synthase 2. *Cell* **83**, 493–501.

[61] Tsujii M, Kawano S, Tsuji S, Sawaoka H, Hori M, and DuBois RN (1998). Cyclooxygenase regulates angiogenesis induced by colon cancer cells. *Cell* **93**, 705–716.

[62] Kanaoka S, Yoshida K, Miura N, Sugimura H, and Kajimura M (2004). Potential usefulness of detecting cyclooxygenase 2 messenger RNA in feces for colorectal cancer screening. *Gastroenterology* **127**, 422–427.

[63] Takai T, Kanaoka S, Yoshida K, Hamaya Y, Ikuma M, Miura N, Sugimura H, Kajimura M, and Hishida A (2009). Fecal cyclooxygenase 2 plus matrix metalloproteinase 7 mRNA assays as a marker for colorectal cancer screening. *Cancer Epidemiol Biomarkers Prev* **18**, 1888–1893.

[64] Lahm H, Petral-Malec D, Yilmaz-Ceyhan A, Fischer JR, Lorenzoni M, Givel JC, and Odartchenko N (1992). Growth stimulation of a human colorectal carcinoma cell line by interleukin-1 and -6 and antagonistic effects of transforming growth factor β1. *Eur J Cancer* **28A**, 1894–1899.

[65] Enss ML, Cornberg M, Wagner S, Gebert A, Henrichs M, Eisenblatter R, Beil W, Kownatzki R, and Hedrich HJ (2000). Proinflammatory cytokines trigger MUC gene expression and mucin release in the intestinal cancer cell line LS180. *Inflamm Res* **49**, 162–169.

[66] Jarry A, Vallette G, Branka JE, and Laboisse C (1996). Direct secretory effect of interleukin-1 via type I receptors in human colonic mucous epithelial cells (HT29-C1.16E). *Gut* **38**, 240–242.

[67] Plaisancie P, Barcelo A, Moro F, Claustre J, Chayvialle JA, and Cuber JC (1998). Effects of neurotransmitters, gut hormones, and inflammatory mediators on mucus discharge in rat colon. *Am J Physiol* **275**, G1073–G1084.

[68] Yu YJ, Majumdar AP, Nechvatal JM, Ram JL, Basson MD, Heilbrun LK, and Kato I (2008). Exfoliated cells in stool: a source for reverse transcription–PCR–based analysis of biomarkers of gastrointestinal cancer. *Cancer Epidemiol Biomarkers Prev* **17**, 455–458.

[69] Van Lieshout EM, Van Doesburg W, and Van der Meer R (2004). Real-time PCR of host DNA in feces to study differential exfoliation of colonocytes between rats and humans. *Scand J Gastroenterol* **39**, 852–857.

[70] Shattuck-Brandt RL, Varilek GW, Radhika A, Yang F, Washington MK, and DuBois RN (2000). Cyclooxygenase 2 expression is increased in the stroma of colon carcinomas from IL-10(–/–) mice. *Gastroenterology* **118**, 337–345.

[71] Sohn KJ, Shah SA, Reid S, Choi M, Carrier J, Comiskey M, Terhorst C, and Kim YI (2001). Molecular genetics of ulcerative colitis–associated colon cancer in the interleukin 2– and β(2)-microglobulin–deficient mouse. *Cancer Res* **61**, 6912–6917.

[72] Rudolph U, Finegold MJ, Rich SS, Harriman GR, Srinivasan Y, Brabet P, Boulay G, Bradley A, and Birnbaumer L (1995). Ulcerative colitis and adenocarcinoma of the colon in $G_{\alpha i2}$-deficient mice. *Nat Genet* **10**, 143–150.